Academic Sciences International Journal of Pharmacy and Pharmaceutical Sciences

ISSN- 0975-1491 Vol 6, Issue 1, 2014

Reserch Article

INDOMETHACIN LOADING AND *IN VITRO* RELEASE PROPERTIES FROM VINYL ACETATE HOMO- AND CO-POLYMER NANOPARTICLES, COATED WITH POLYZWITTERION AND CARBOPOL® SHELLS

VELICHKA ANDONOVA[1]*, GEORGE GEORGIEV[2], VENCISLAVA TONCHEVA[2], NADIA PETROVA[3], DANIELA KARASHANOVA[4], DIMITAR PENKOV[1], MARGARITA KASSAROVA[1]

[1] Department of Pharmaceutical Sciences, Faculty of Pharmacy, Medical University Plovdiv, Plovdiv 4000, [2] Faculty of Chemistry and Pharmacy, Sofia University "St. Kliment Ohridski", Sofia, [3]Institute of Mineralogy and Crystallography, Bulgarian Academy of Sciences, Sofia, [4] Institute of Optical Materials and Technologies "Acad. Jordan Malinovski", Bulgarian Academy of Sciences, Sofia, Bulgaria. Email: andonova_v@abv.bg

Received: 13 Nov 2013, Revised and Accepted: 09 Dec 2013

ABSTRACT

Objective: To examine indomethacin (IMC) inclusion in *in-situ* loaded nanoparticles (IMC-NPs) and its *in vitro* release characteristics varying the polymer composition of the NPs cores and shells.

Methods: IMC-NPs were obtained by emulsifier-free radical homo- and co-polymerization of the monomers in the presence of IMC. Poly(vinyl acetate) (pVAc) and a copolymer of vinyl acetate (VAc) with 3-dimethyl(methacryloyloxyethyl) ammonium propane sulfonate (DMAPS), (p(VAc-co-DMAPS), were used for the preparation of NPs cores, while biocompatible poly(DMAPS), (pDMAPS), and Carbopol® (Cbp) were used for the preparation of the NPs shells. TEM and DLS were used to observe the microstructure and determine the particle size. XRD-, FTIR-, UV-spectroscopy and simultaneous DTA-TG analysis were applied for the determination of IMC inclusion and *in vitro* release characteristics.

Results: TEM and DLS determined the particle size which was in range of 128.10÷345.10 nm and its polydispersity index within 0.133÷0.390. A monomodal particle size distribution was observed for the homo- and copolymer uncoated NPs. Bimodal distribution was observed for the coated with pDMAPS and Cbp NPs. Drug loading assessment showed higher values for drug loading, encapsulation efficiency and NPs yield for the uncoated NPs compared to those which were coated with Cbp or pDMAPS. Results of release kinetic analyses showed that IMC was released from investigated patterns following first order kinetics, but their release rate and degree were different. The copolymer NPs (IMC-p(VAc-co-DMAPS)) showed the most rapid release of IMC, while the homopolymer pVAc NPs, coated with Cbp (IMC-p(VAc)+Cbp) - the slowest one.

Conclusion: The obtained results prove the possibility to prepare pVAc and p(VAc-co-DMAPS) NPs with *in-situ* included IMC by emulsifier-free radical homo- and co-polymerization and demonstrate the importance of polymer nature and NPs cores and shells composition for the control of IMC loading and release characteristics.

Keywords: Indomethacin-loaded nanoparticles, Radical polymerization, Polyzwitterion coated nanoparticles, Carbopol coated nanoparticles, Vinyl acetate homo- and co-polymers.

INTRODUCTION

Indomethacin (IMC), ([1-(4-chlorobenzoyl)-5-methoxy-2-methylindol-3-yl]-acetic acid) is a nonsteroidal anti-inflammatory drug that is used to treat osteoarthritis, rheumatoid arthritis, bursitis, tendinitis, gout, ankylosing spondylitis and headache [1]. It is practically insoluble in water, unstable in alkaline and acidic media and slightly soluble in alcohol [2]. Due to its properties, drug formulations that contain IMC often show low and erratic bioavailability, and for oral use there is increasing irritation of the stomach lining due to prolonged contact with it [3, 4]. In ophthalmology, IMC is used as topical eye drops for prevention of miosis during cataract surgery, cystoid macular edema and conjunctivitis [1, 5]. Its use in liquid formulations is limited due to its insolubility in water, low bioavailability and ocular mucosa irritation.

In the last decade, researchers define the use of NPs of biocompatible and biodegradable polymers as an effective drug-release system, which aim is to increase solubility and bioavailability, and reduce the irritating effects of the drug [6]. In order to overcome the technological problems associated with IMC insolubility and instability in aqueous medium and its low bioavailability following topical application, various models of drug-delivery systems have been developed. IMC has been included into nanosuspensions [7, 8], microemulsions [7, 9], polymeric NPs [6, 10, 11]. The authors used different methods and a huge variety of excipients to increase solubility, improve bioavailability and reduce the drug side effects. For example, NPs based on copolymers of methyl methacrylate and glycidyl methacrylate with IMC [10] have been developed via emulsion radical polymerization. Studies on NPs of cyclodextrin with IMC have also been performed [11].

On the other hand, pVAc latex and VAc copolymer latexes are of a great importance in industrial and scientific aspects [12]. The reaction conditions play a crucial role on the emulsion polymerization. The properties of the produced copolymers are a result of the significant differences between the properties of VAc and other comonomers [12, 13, 14]. In our previous study we have demonstrated the possibility of *in-situ* inclusion of IMC in pVAc and polystyrene NPs using emulsifier-free radical polymerization of monomers [15] and have selected the best conditions for this process [16].

The purpose of this study was to investigate the influence of the nature and composition of the monomer feed, added to the reaction system (IMC/VAc/comonomer) and the characteristics of the obtained polymer latexes on IMC *in-situ* loading and its kinetic release properties.

Kostova et al. have synthesized zwitterionic copolymers, p(VAc-co-DMAPS), characterized metoprolol tartrate delivery from tablets, based on these copolymers, and investigated the morphology and microstructure of the same tablets [17, 18].

The original contribution of the presented work is the *in-situ* drug (IMC) inclusion in the pVAc and p(VAc-co-DMAPS) nanosized latexes, and the established release IMC characteristics from these NPs. In addition, it was proved that the NPs coating with polymer shells opened new possibilities for the control of the IMC release characteristics. These results confirm literature data [19, 20, 21]

demonstrating that NPs coating not only affects the release kinetics, but also reduces the side effects of certain drugs.

MATERIALS AND METHODS

In this research IMC as a drug and vinyl acetate (VAc) as a monomer were purchased from Fluka. Potassium dihydrogen phosphate and *di*-sodium hydrogen phosphate from Merck (Darmstadt, Germany) were used for the preparation of a phosphate-phosphate buffer (Sorensen's phosphate buffer) (PPB). 3-dimethyl (methacryloyloxyethyl) ammonium propane sulfonate (DMAPS) from Merck (Darmstadt, Germany) was used to obtain poly(VAc-co-DMAPS) (p(VAc-co-DMAPS) and poly(3-dimethyl (methacryloyloxyethyl) ammonium propane sulfonate), (pDMAPS). Ammonium persulfate (AP), (Fluka) was used as an initiator. Carbopol 971 (BF Goodrich, Cleveland, OH) was used as a polymer for the preparation of IMC-NPs.

Preparation of IMC-loaded nanocarriers

IMC-loaded nanoparticles (IMC-NPs) were obtained by an emulsifier-free radical polymerization of the monomers (v/v), in the presence of IMC 1% (w/v). The polymerization was conducted in a nitrogen atmosphere and a temperature of 55°C, for 90 min under ultrasonic impact (Ultrasonicator Siel UST7.8-200, Gabrovo, Bulgaria). Ammonium persulphate (AP) in concentration 1% (w/v) was used as initiator. The model latexes were exposed at dialysis through membrane with MWCO 8000 Da for 7 h to eliminate the low molecular weight compounds (e.g. the initiator of process, residual monomers or free IMC) from the primary latex, and then the samples were freeze-dried [15, 16]. In Table 1 the investigated models and the method of their preparation are shown.

Table 1: Investigated models and method of their preparation

Model	Preparation method
IMC-pVAc	Emulsifier-free emulsion polymerization of VAc 10% (v/v) in the presence of IMC 1% (w/v) in water.
IMC-p(VAc-co-DMAPS)	Emulsifier-free emulsion copolymerization of VAc and DMAPS (moll ratio 1:1) in the presence of IMC 1% (w/v) in water.
IMC-p(VAc)+pDMAPS	Emulsifier-free emulsion polymerization of VAc 10% (v/v) in the presence of IMC 1% (w/v) in aqueous solution of pDMAPS 1% (w/v).
IMC-p(VAc)+Cbp	Emulsifier-free emulsion polymerization of VAc 10% (v/v) in the presence of IMC 1% (w/v) in aqueous solution of Cbp 1% (w/v).
IMC-p(VAc-co-DMAPS)+Cbp	Emulsifier-free emulsion copolymerization of VAc and DMAPS (moll ratio 1:1) in the presence of IMC 1% (w/v) in aqueous solution of Cbp 1% (w/v).

Synthesis of pDMAPS

p(DMAPS) was obtained by radical homopolymerization in water with AP as an initiator (1%, w/v) and monomer concentration 12% (w/v). The polymerization was carried out in an air atmosphere, stirring continuously and at 50°C. The time of the polymerization was 6 h. The resulting p(DMAPS) was precipitated in acetone, washed three times with water-alcohol mixture (1/1, v/v) and then redissolved in water and precipitated in acetone. Precipitated polymer was dried at 40°C to a constant mass. It was characterized with NMR, IR spectroscopy and elemental analysis.

Characterization of NPs

Transmission electron microscopy (TEM)

TEM images of the investigated models were produced by transmission electron microscope JEOL JEM 2100 (JEOL Ltd., Japan) with accelerating voltage 200 kV. For the phase identification of the samples the diffraction mode of the microscope, Selected area electron diffraction (SAED), was used. The following preparation procedure was applied before the observation of the samples in the microscope: micro-quantities of the studied substance were mixed with distilled water in a test tube and placed in an ultrasonic bath to homogenise for 3 min. Thereafter, the suspension was dropped on carbon-coated standard Cu grid and dried under air conditions in a dust free environment for 24 h.

X-ray powder diffraction (XRD)

XRD was made by using of X-ray powder diffractometer D2 Phaser (Bruker AXS GmbH, Karlsruhe, Germany) with Ni-filtrated Cu x-ray radiation in average 4–60° 2-theta under conditions 30 kV and 10 mA.

Fourier transforms infrared spectroscopy (FTIR)

FTIR was carried out with FTIR Bruker Tensor 37 Spectrometer (Bruker Optics GmbH, Germany), using the technique of tableting with KBr and resolution 2 cm^{-1} at 120 scans for each sample.

Thermal analysis (DTA-TG)

The simultaneous DTA-TG analysis was performed on the apparatus Stanton Redcroft STA-780 under the following experimental conditions: heating the samples from room temperature up to 600°C, weight of sample - 10 mg; heating rate - 10°C/min and blower atmosphere of Ar (20 ml/min).

Particle size distribution (PSD) and zeta potential (ζP) analysis

PSD of tested models were determined through dynamic light scattering (DLS, Zetasizer Nano ZS, Malvern Instruments, Malvern, UK) in measurement range of 0.3 nm – 10 μm (diameter), minimum sample volume 12 μl. The samples were prepared using equal quantity of NPs in Sorensen's phosphate buffer at pH 7.4 (PPB) and filtered through a filter Chromafil Xtra 0.45 μm before measuring the particle mean diameter and polydispersity index (PDI). **ζ**P of NPs were also measured under the same conditions using the principle of electrophoretic light scattering at the same apparatus Zetasizer Nano ZS with specifications: light source He-Ne laser 632.8 nm, 4 mV and backscatter detection at 173°. The experiments were repeated three times and the results were calculated as mean values ± SD (SD – standard deviation).

Drug loading and *in vitro* release studies

Drug loading assessment

To determine the amount of incorporated IMC into the NPs, 2.5 mg of IMC-loaded NPs were weighted and dissolved in 25.0 ml methanol and placed under ultrasonic impact (Ultrasonicator Siel UST7.8-200, Gabrovo, Bulgaria) for 90 min. The quantitative defining of IMC was made spectrophotometrically at λ=320 nm with UV/VIS spectrophotometer Ultrospec 3300 (Biochrom Ltd., Cambridge, UK) after filtering the samples through a filter Chromafil Xtra 0.45 μm. Control experiments were performed for any absorbance using blank NPs without IMC. The measurements were made compared to the medium of examination. The total drug content of each formulation was calculated from the standard curve (with a linearity coefficient (r) = 0.999). Each experiment was repeated six times and the results were presented as means ± SD. The drug loading (%DL), encapsulation efficiency (%EE) and NPs yield (%Y) were calculated using the following equations:

$$\%DL = \frac{\text{Weight of IMC entrapped within NPs}}{\text{Total weight of NPs}} \text{x} 100 \quad (1)$$

$$\%EE = \frac{\text{Weight of IMC entrapped within NPs}}{\text{Total IMC added}} \text{x} 100 \quad (2)$$

$$\%Y = \frac{\text{Total weight of NPs}}{\text{Weight of polymer} + \text{weight of IMC}} \text{x} 100 \quad (3)$$

***In vitro* Release of IMC from IMC-NPs**

Examination on the release of IMC from the model nanosized particles was carried out in a thermostated vessel with equal amounts of the tested models under perfect "sink" conditions; working volume for dissolution 100.0 ml Sorensen's PPB at pH 7.4; temperature 37°C±0.5°C; stirring speed 100 min^{-1}. The quantitative defining of IMC was made spectrophotometrically at λ=320 nm on UV/VIS spectrophotometer Ultrospec 3300 pro (Biochrom Ltd., Cambridge, UK) after filtering the samples through a filter Chromafil Xtra 0.45 μm. The measurements were made compared to the medium of examination Sorensen's PPB at pH 7.4. Control experiments were performed using NPs without IMC. The experiments were repeated six times, the results were presented as mean values. The concentrations were calculated from the standard curve with a linearity coefficient (r) = 0.999.

RESULTS

Characterization of NPs

TEM

Figure 1 shows TEM micrographs of the investigated models. The particles of the observed samples differ in size and shape. The smallest particle dimensions were established at model IMC-pVAc (Figure 1a). This can be explained with the hydrophobic character of pVAc carrier and used IMC. In the model IMC-p(VAc-co-DMAPS) (Figure 1b) were observed particles with sizes, greater than those of IMC-pVAc, due to the presence of hydrophilic DMAPS monomer units in the copolymer macromolecule. In both cases, the particles have spherical shape with diameters less than 100 nm as opposed to the "flower – like" particles of IMC-p(VAc)+pDMAPS, with size about 50-75 nm, presented on Figure 1c. Adding 1% aqueous solution of Cbp to models IMC-p(VAc)+Cbp (Figure 1d) and IMC-p(VAc-co-DMAPS)+Cbp (Figure 1e) led to NPs with dimensions around 50 nm and less, coated with Cbp. The formation of polymeric shell around the particles is demonstrated on the micrographs. The particles have regular spherical shape and different contrast, which is a testament to the different particle density. In model IMC-p(VAc-co-DMAPS)+Cbp (Figure 1e) the darkest particles are probably pVAc-NPs with higher content of IMC, while the lighter ones are homopolymers of DMAPS and copolymers of VAc with DMAPS. Contrary to the results from XRD of this sample, the SAED patterns demonstrate crystalline structure. It is noteworthy that the SAED is a method for determination of a local structure, while XRD is for integral one. The electron diffraction can identify micro-quantities of crystalline phase distributed in amorphous matrix, which is the case of sample IMC-p(VAc-co-DMAPS)+Cbp (Figure 1e). In all models the NPs tend to aggregate. Some of them (IMC-pVAc and IMC-p(VAc-co-DMAPS)) have a characteristic conformation, resulting in a crystalline structure, demonstrated on the SAED patterns (Figure 1f). This effect can be explained by the crystallization of IMC itself, included in the nanosized particles, as it is confirmed by the XRD analysis.

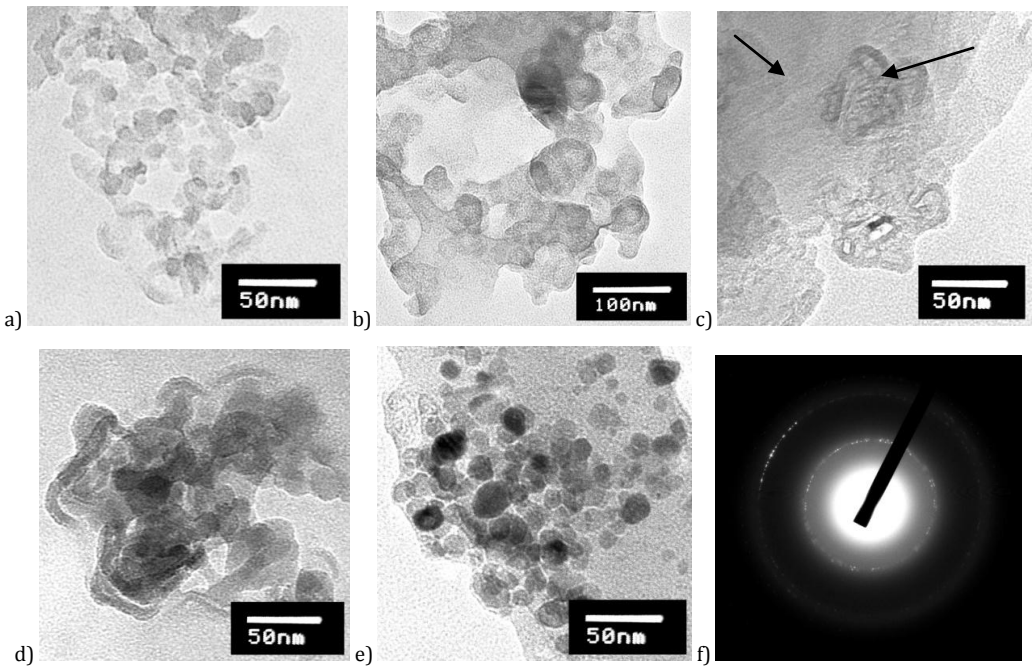

Fig. 1: TEM of (a) IMC-pVAc, (b) IMC-p(VAc-co-DMAPS), (c) IMC-p(VAc)+pDMAPS, (d) IMC-p(VAc)+Cbp, (e) IMC-p(VAc-co-DMAPS)+Cbp, and (f) electron diffraction of IMC-pVAc.

XRD analysis

XRD was made on all of the investigated models and the results were compared to those of pure IMC. Figure 2 shows XRD of pure IMC which was compared to the same of the investigated samples. In the investigated IMC-pVAc, IMC-p(VAc-co-DMAPS), IMC-p(VAc) + pDMAPS, IMC-p(VAc)+Cbp models the crystalline substance is only IMC. The relative content of IMC is greater in IMC-p(VAc-co-DMAPS) and IMC-p(VAc)+Cbp compared to IMC-p(VAc)+pDMAPS model, while the model IMC-p(VAc-co-DMAPS)+Cbp shows amorphous structure and contains no crystalline IMC [22].

FTIR analysis

Figure 3 shows the IR-spectra of the investigated models compared to the pure IMC and pVAc-NPs without IMC as a blank. In the spectrum of pure IMC (γ–type is more stable and less soluble polymorphic modification of IMC in comparison with α-modification) two most intensive peaks, at 1717 cm^{-1} and at 1690 cm^{-1} of υC=O, are shown [23]. Spectra of IMC-pVAc, IMC-p(VAc-co-DMAPS) and IMC-p(VAc)+Cbp models show a similarity with this of pure IMC [23, 24]. Obviously, in the current systems there is no covalent interaction between polymers and IMC, but the interaction between them by hydrogen bonds [24] is possible. In the spectra of IMC-p(VAc)+pDMAPS and IMC-p(VAc-co-DMAPS)+Cbp there are the characteristic absorption peaks of IMC, but their intensity is much lower than those in the spectra of pure IMC and the other investigated models. The reason for this may be the lower quantity of incorporated IMC in these NPs.

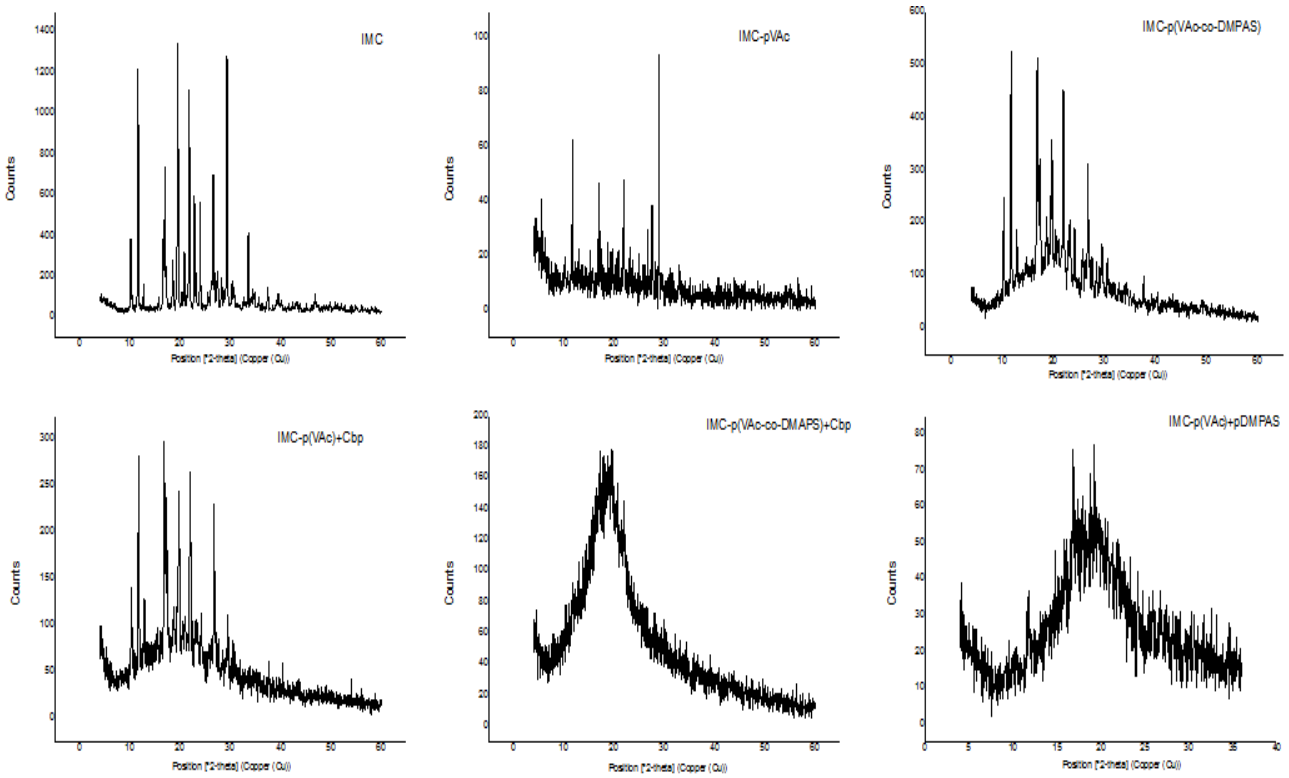

Fig. 2: XRD of pure IMC, compared to the patterns IMC-pVAc, IMC-p(VAc-co-DMAPS), IMC-p(VAc)+Cbp, IMC-p(VAc-co-DMAPS)+Cbp and IMC-p(VAc)+pDMAPS.

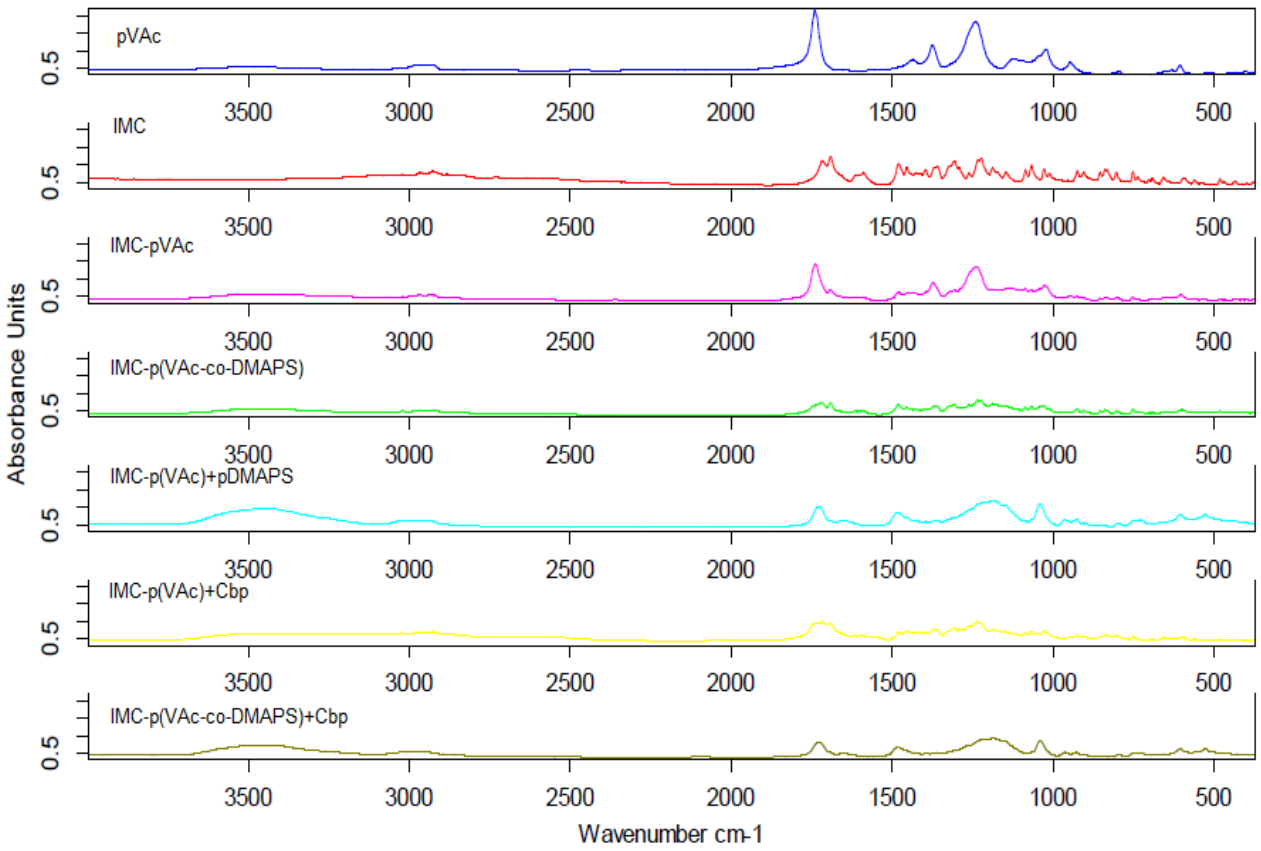

Fig. 3: FTIR-spectra of pVAc, IMC, IMC-pVAc, IMC-p(VAc-co-DMAPS), IMC-p(VAc)+pDMAPS, IMC-p(VAc)+Cbp and IMC-p(VAc-co-DMAPS)+Cbp.

DTA-TG analysis

The results from the thermal analysis of IMC and pVAc (as a blank NPs without IMC) are shown in Figure 4 and about IMC-pVAc, IMC-p(VAc-co-DMAPS) and IMC-p(VAc)+Cbp models - in Figure 5. The first endothermic peak of DTA-curves of IMC (Figure 4a) is associated with a melting process and does not correspond to a weight loss of the TG-curve (Figure 4b). This peak was found at 168.4^{o}C for IMC and according to the current analysis displacement towards lower temperatures (162.6, 166.1, 167.32^{o}C) respectively for IMC-pVAc, IMC-p(VAc-co-DMAPS) and IMC-p(VAc)+Cbp, was shown (Figure 5a). Such a negligible displacement of the melting point is another proof of the absence of chemical interaction between the polymeric carrier and IMC [25, 26]. Endothermic effect at 87.1^{o}C for the IMC-p(VAc)+Cbp model was related to minor weight loss and due to the release of the physically adsorbed water. The main decomposition of the model carriers was in the 230 – 450^{o}C temperature interval (expressed in a series of endothermic reactions) and it was linked to the release of volatile components reflecting on the TG-curves (Figure 5b). The loss of weight was one-stage and almost 100% in the case of IMC, while in the case of pVAc-blank NPs there were two-stages and did not reach 100% in the investigated temperature interval (Figure 4b). The weight loss was also two- or more-stages for IMC-pVAc, IMC-p(VAc-co-DMAPS) and IMC-p(VAc)+Cbp models and did not reach 100% up to 600^{o}C (Figure 5b). The evolution of TG- and DTA-curves shows a greater similarity between IMC (Figure 4) and IMC-pVAc (Figure 5). In the case of the other models (IMC-p(VAc-co-DMAPS) and IMC-p(VAc)+Cbp) the thermal evolution becomes more complicated in comparison with IMC.

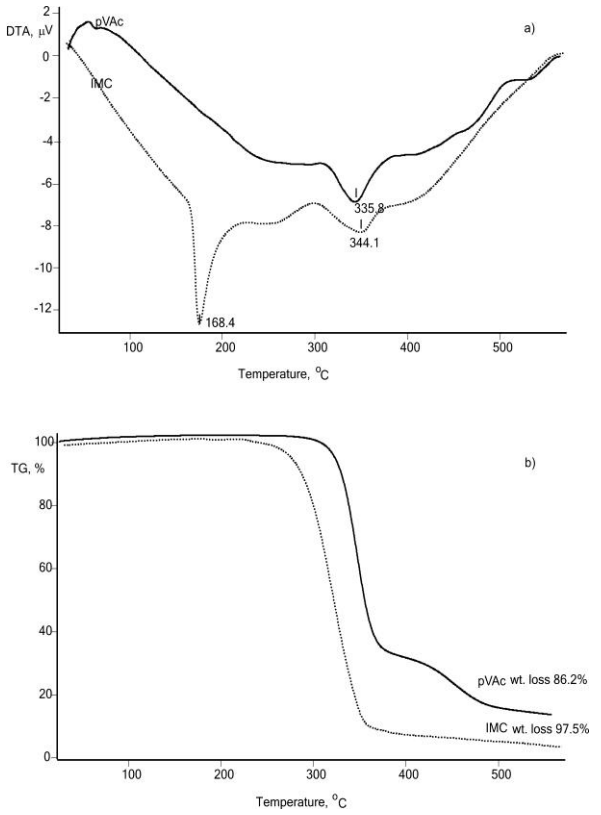

Fig. 4: DTA-curves (a) and TG-curves (b) of IMC and pVAc samples.

PSD and ζP analysis

The results of the PSD are presented in Figure 6 and **ζ**P, polydispersity index (PDI) and average particle size (Z-average) are presented on Table 2. Highest levels of **ζ**P have been measured for IMC-pVAc and IMC-p(VAc)+Cbp models. **ζ**P absolute values over 30 are the criteria for relative physical stability of the system [27, 28]. As the absolute value of **ζ**P is lower (for IMC-p(VAc)+pDMAPS, IMC-p(VAc-co-DMAPS), IMC-p(VAc-co-DMAPS)+Cbp) models) the possibilities for an aggregation among the particles are larger. The equal values of **ζ**P for the IMC-pVAc and IMC-p(VAc)+Cbp models were probably due to the greater quantity of included IMC into IMC-pVAc, whose negatively charged groups led to close values of the **ζ**P as that for the IMC-p(VAc)+Cbp model, formed by the coating of NPs with Cbp. Significantly lower levels of **ζ**P on the models, involved DMAPS monomer (or pDMAPS), were probably due to the zwitterionic character of DMAPS, having positively charged ($C_4H_{10}N^+$) and negatively charged (SO_3^-) groups.

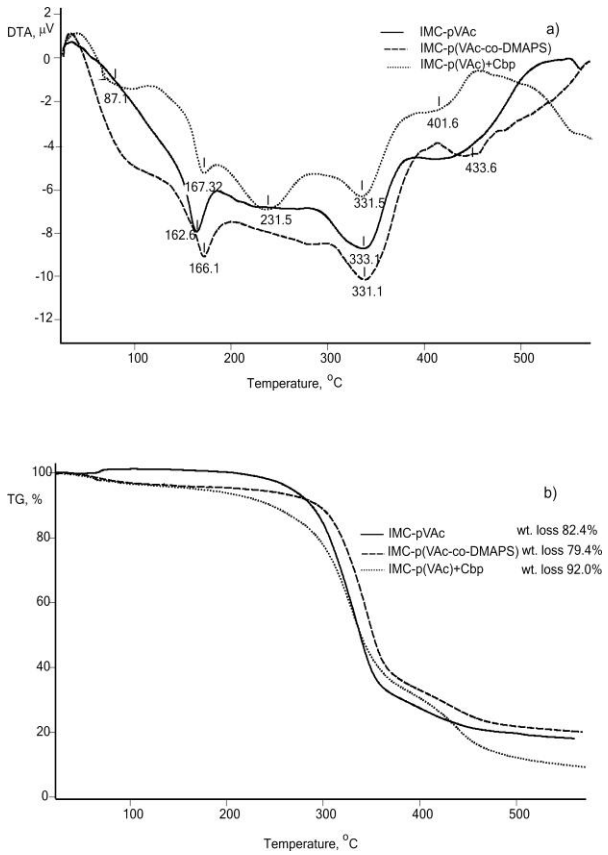

Fig. 5: DTA-curves (a) and TG-curves (b) of IMC-pVAc, IMC-p(VAc-co-DMAPS) and IMC-p(VAc])+Cbp models.

Models IMC-pVAc (Figure 6a) and IMC-p(VAc-co-DMAPS) (Figure 6b) had monomodal PSD. For these models the lowest values of PDI were observed: 0.133 for IMC-pVAc and 0.198 for IMC-p(VAc-co-DMAPS). For models IMC-p(VAc)+pDMAPS, IMC-p(VAc)+Cbp and IMC-p(VAc-co-DMAPS)+Cbp (Figures 6c - 6e) bimodal PSD with higher PDI and larger average of particle size were observed. About 20% of the particles of IMC-p(VAc)+pDMAPS and IMC-p(VAc-co-DMAPS)+Cbp models were at size around 20 nm. In the IMC-p(VAc)+Cbp model about 5% of the NPs were in area 2 from bimodal PSD with size around 35 nm. Bimodal particle size distribution for the models, obtained in the presence of pDMAPS or Cbp can be related to the shell formation around the particles. A part of them remained uncoated, due to insufficient amount of the polymer, and demonstrated a small size. The higher average particle size determined by DLS analysis in comparison with those from TEM was a result of the sample swelling in an aqueous environment. This swelling was the greatest in IMC-p(VAc-co-DMAPS)+Cbp model.

Table 2: Zeta potential (ζP), polydispersity index (PDI) and average particle size (Z-average) of IMC-PVAc, IMC-p(VAc-co-DMAPS), IMC-p(VAc)+pDMAPS, IMC-p(VAc)+Cbp and IMC-p(VAc-co-DMAPS)+Cbp (n=3)

Model	ζP ± SD, (mV)	PDI	Z-average ± SD, (nm)
IMC-pVAc	-31.5±1.2	0.133	128.1±3.4
IMC-p(VAc-co-DMAPS)	-12.5±0.3	0.198	142.1±2.5
IMC-p(VAc)+pDMAPS	-7.65±0.5	0.377	191.6±2.3
IMC-p(VAc)+Cbp	-31.5±2.3	0.224	197.5±3.9
IMC-p(VAc-co-DMAPS)+Cbp	-16.3±1.8	0.390	345.1±3.6

Drug loading and *in vitro* release studies

Drug loading assessment

The results of the investigation of IMC loading in NPs are presented in Table 3. Data show higher values for %EE, %DL and %Y for the uncoated NPs compared to those, coated with Cbp or pDMAPS. IMC-p(VAc)+Cbp model is with lower %Y, but with higher for %EE and %DL values, in contrast to model IMC-p(VAc)+pDMAPS. The nature of polymers (pDMAPS or Cbp) is the main reason for this. Probably, a part of IMC was dissolved in the aqueous solution of polyzwitterionic polymer pDMAPS. A quantity thereof was included on the surface of the particle, and a portion remained dissolved in the medium and was eliminated during the dialysis. The addition of DMAPS monomer and Cbp in the solution for the preparation of IMC-p(VAc-co-DMAPS)+Cbp model increased the viscosity of the aqueous medium and this complicated the process of polymerization, and IMC was probably included in NPs during their formation.

Table 3: Encapsulation efficiency (%EE), drug loading (%DL), and NPs yield (%Y) (n=6)

Model	%EE±SD	%DL±SD	%Y±SD
IMC-pVAc	82.92±1.01	7.67±0.32	98.32±1.33
IMC-p(VAc-co-DMAPS)	75.58±0.77	7.16±0.65	96.02±1.09
IMC-p(VAc)+Cbp	47.56±0.51	4.49±0.23	88.32±1.23
IMC-p(VAc)+pDMAPS	36.62±0.84	3.22±0.54	94.89±1.45
IMC-p(VAc-co-DMAPS)+Cbp	6.81±0.33	0.72±0.16	79.03±1.08

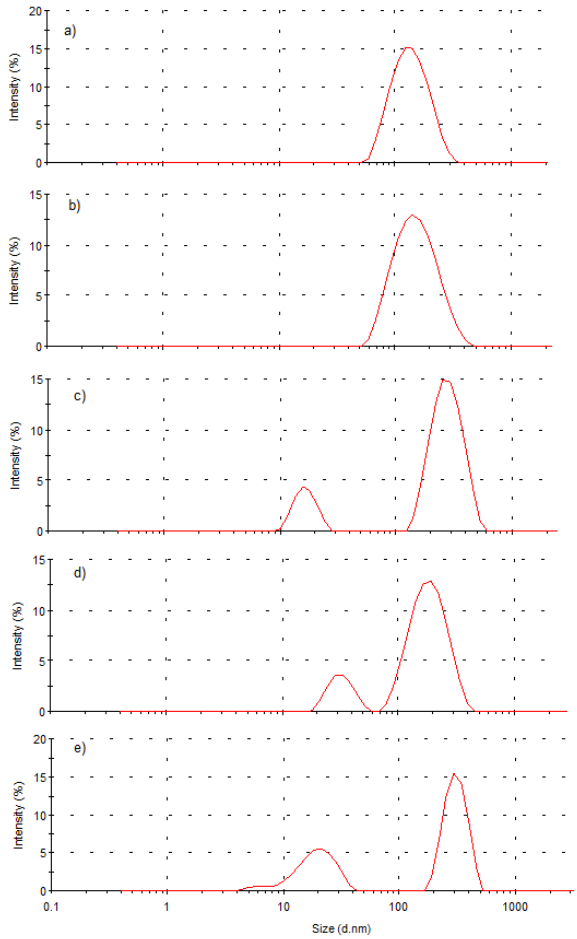

Fig. 6: Particle size distribution (PSD) for models (a) IMC-pVAc, (b) IMC-p(VAc-co-DMAPS), (c) IMC-p(VAc)+pDMAPS, (d) IMC-p(VAc)+Cbp, and (e) IMC-p(VAc-co-DMAPS)+Cbp.

***In vitro* release of IMC from IMC-NPs**

Figure 7 presents the release profiles of IMC included in the carriers IMC-pVAc, IMC-p(VAc-co-DMAPS), IMC-p(VAc)+pDMAPS and IMC-p(VAc)+Cbp. The results are presented as a percentage of the included into NPs IMC. The IMC-p(VAc-co-DMAPS)+Cbp profile is not presented because the recent analyses (XRD, FTIR) showed that the model did not contain crystalline IMC (only 6.81% as %EE, Table 3). The blank formulation had not any significant absorbance at 320 nm.

Model IMC-pVAc released 70% of the entrapped drug for 1.5 h from the start, while 7 h afterward this percentage was 99% (Figure 7). The fastest IMC release demonstrated the IMC-p(VAc-co-DMAPS) model. After 15 min from the start it released 52%, after 1 h - 85%, and after 1.5 h - 94% of the entrapped drug. The speed and the degree of release in this case depended on the copolymer composition, more exactly on the mole fraction of the DMAPS monomer units, increasing the hydrophilicity of the p(VAc-co-DMAPS) carrier in comparison with other models. During the preparation of the IMC-p(VAc)+pDMAPS model, a part of IMC was dissolved in the aqueous polyzwitterion solution. Therefore, the included in the NPs shell IMC should be released at first. Indeed, this model released 45% of the included IMC for 45 min only. Another drug part, included in the pVAc, and connected via weak hydrogen bonds with pVAc matrix, released slowly and 94% IMC was released for 2.5 h.

The slowest IMC release, established for IMC-p(VAc)+Cbp model, was related to the hydrophobic nature of pVAc-NPs, coated with the hydrophilic Cbp. The swelling Cbp shell retarded the water deliver to the pores of the hydrophobic pVAc core, as a result of which only 56% of the included drug was released within 16 h.

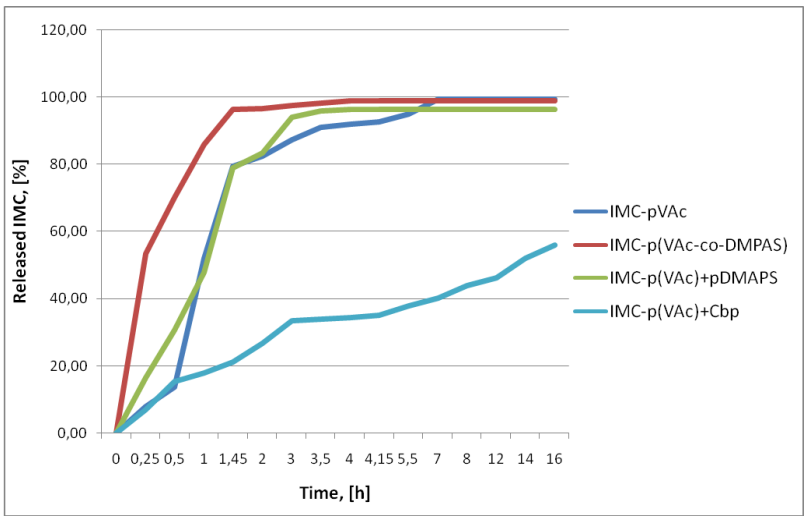

Fig. 7: IMC release profiles from IMC-pVAc, IMC-p(VAc-co-DMAPS), IMC-p(VAc)+pDMAPS and IMC-p(VAc)+Cbp models.

To determine the kinetic model that best describes the release mechanism, the *in vitro* release data were analyzed according to zero-, first- and Higuchi models. The model with the highest correlation coefficient (R^2) was selected as the best fit [19]. The obtained results show that IMC release from all investigated patterns follows the first order release kinetics (Table 4). These results relate to conditions in which there is no change in the shape of the NPs during the dissolution process (i.e. the surface area remains constant) [29]. Based on the higher values of R^2 for the Higuchi model it is possible to determine the drug transport mechanism as Fickian diffusion [30].

Table 4: Correlation coefficient (R^2) values of different kinetic models for the IMC release from IMC-NPs

Formulation	Correlation Coefficient (R^2)		
	Zero	First	Higuchi
IMC-pVAc	0,612	0,962	0,869
IMC-p(VAc-co-DMAPS)	0,392	0,991	0,946
IMC-p(VAc)+pDMAPS	0,798	0,975	0,946
IMC-p(VAc)+Cbp	0,902	0,993	0,987

DISCUSSION

Macroscopically, traditional amorphous polymeric materials have no preferred shape. Individual polymer molecules generally adopt an isotropic "random coil" conformation in melt or solution, as the "flower – like" particles of IMC-p(VAc)+pDMAPS, with size about 50-75 nm, presented on Figure 1c. The formation of these structures could be related to the mixture of separately polymerized components – pVAc and pDMAPS. Hence, polymer particles are spherical in shape as a result of minimizing surface tension [31]. A polyelectrolyte, in low ionic strength solutions, tends to be in its most extended uncoiled form due to the intramolecular repulsion on the unscreened charges on each monomeric unit of the macromolecule [32]. In dilute solutions, pDMAPS macromolecular chains are not connected to each other and exist as separate polymer coils [33]. The increase of the polymer concentration during the freeze-drying induces the interaction between macromolecular chains as a result of which NPs with different shape are obtained (Figure 1c). The XRD analysis demonstrated the crystallization, observed by SAED in some of IMC-loaded NPs, which could be related to the IMC crystallization, incorporated into NPs. The structure of the IMC-NPs depended on the quantity of the included IMC. This result was confirmed by FTIR and DTA-TG analysis. They proved the absence of a covalent interaction between polymer chains and IMC but presence of interaction via hydrogen bonds [24]. The similarity of IR-spectrum of pure IMC with those on the investigated models depended on the quantity of the included IMC and proved the IMC inclusion in NPs.

IMC-pVAc model showed monomodal PSD, low value for PDI and **ζ**P providing relative stability of the system. Both the drug and the carrier have hydrophobic properties and this is the model with the higher content of included IMC – 7.67%. This model released 99% of the included IMC for 7 h. A possible reason for this result could be

the formation of pores in the pVAc matrix during the extraction of the residual monomer and the initiator from NPs. The more complete the extraction of these compounds from the matrix was, the more pores were formed, which allowed a complete release of IMC incorporated in the matrix.

The addition of monomer units with a quite different hydrophilicity (zwitterionic, DMAPS ones) than that of VAc ones changed the NPs **ζ**P, the amount of included drug (7.16%) and the releasing rate. After 1.5 h 94% from the entrapped IMC was released. This was a result of the hydrophilic properties of DMAPS monomer units. Water more easily penetrated into the matrix and dissolved the drug, which then diffused into the exterior medium.

The inclusion of aqueous polymer solution during the polymerization led to the coating of IMC-pVAc-NPs with a shell from this polymer. Its physicochemical properties had an impact on the characteristics of the NPs. Adding both polymers (pDMAPS or Cbp) led to bimodal PSD. The values of **ζ**P depended on the polymer nature: for IMC-p(VAc)+pDMAPS this value was -7.65 mV, while for IMC-p(VAc)+Cbp the value was -31.5 mV, because Cbp is anionic polymer. There has been a difference in the amount and the rate of the IMC release. IMC-p(VAc)+pDMAPS model was loaded with 3.22% IMC, and 94% of it was released for 2.5 h. During the preparation of the IMC-p(VAc)+pDMAPS model, a part of IMC was dissolved in the aqueous polyzwitterion solution. Therefore, a part of IMC was included in the particle shell, and should be released at first. Indeed, IMC-p(VAc)+pDMAPS released 45% from the included IMC for 45 min only. A part of the dissolved drug in pDMAPS was entrapped in pVAc-core and connected via weak hydrogen bonds with pVAc. pDMAPS included inside the NPs in contact with the water swelled and supported the drug release. In this case the IMC release reached 94% for 2.5 h. The IMC-p(VAc)+Cbp model included 4.49% IMC, and 56% of it was released for 16 h. Cbp as a crosslinked polymer network swelled slower, compared to pDMAPS, and as a result of this the IMC release was slower in this case.

The addition of DMAPS and Cbp during the preparation of IMC-p(VAc-co-DMAPS)+Cbp model increased the viscosity of the aqueous medium. As a result of this the polymerization was changed as well as the inclusion of IMC in the formed NPs. Due to the lowest amount of included IMC, this model was out of interest for the release kinetics.

There was no data in the literature about the interaction between IMC and the used monomers and initiator of the polymerization and IMC, as well as about the IMC influence on the stability of the monomer and polymer dispersions in water. The preliminary experiments allowed choosing the emulsion polymerization conditions, excluding chemical modification and degradation of the IMC molecule [15, 16]. On the other hand, the IMC concentration (1% (w/v)) led to minimum coagulate formations during the polymerization with high yield of NPs (Table 3). Even more, stable polymer latexes with included IMC in nanosized latex particles, were produced without the usage of surfactants, an important advantage of this method for a drug formulation. The challenge was to find easily available and feasible technological parameters for the effective control of the IMC release from the polymer NPs. For that purpose two approaches were tested. The first one was based on the IMC inclusion in the copolymer (p(VAc-co-DMAPS)) nanolatex. With the second approach this control was achieved by changes in the composition of polymer mixture (pVA, pDMAPS, Cbp and p(VA-co-DMAPS)) from which the NPs with included IMC were prepared. The obtained results confirm the efficiency of these approaches for the control of the IMC degree of loading, encapsulation efficiency, its release degree and also the rate of release.

CONCLUSION

The physicochemical properties of the drug and the polymer influence the IMC loading, its release from the NPs and the release kinetics. The results from this investigation definitely prove the importance of the properties of the components used in the polymerization system, on the properties and characteristics of the nanocarrier as a drug releasing system. The possibility for the *in-situ* IMC inclusion in the VAc polymer and copolymer latexes was proved. IMC, as a hydrophobic drug, was released from all investigated patterns following first order release kinetics and it relates to conditions in which there is no change in the shape of the NPs during the dissolution process (i.e. the surface area remains constant). The addition of DMAPS monomer units in copolymer p(VAc-co-DMAPS) and Cbp- or pDMAPS- shell around pVAc-core affects the rate and extent of IMC-releasing but does not influence the kinetic model and drug transport mechanism. It was also shown that the composition of the copolymers and polymer mixtures were effective factors for the control latex loading with IMC and its release characteristics. Future investigations will concern the influence of the nature and quantity of other polymers on its controlled release characteristics.

ACKNOWLEDGMENTS

The authors are grateful to the National Science Foundation for their financial support (Project DDVU-02/43).

REFERENCES

1. Sweetman S. Martindale: The complete drug reference, 33d ed. London: Pharmaceutical Press; 2007.
2. Lobenberg R, Amidon GL. Modern bioavailability, bioequivalence and biopharmaceutics classification system; new scientific approaches to international regulatory standards. Eur J Pharm Biopharm 2000; 50 :3 –12.
3. Hirasawa N, Ishise S, Miyata H, Danjo K. Physicochemical characterization and drug release studies of nilvadipine solid dispersions using water-insoluble polymer as a carrier. Drug Dev Ind Pharm 2003; 29 :339-44.
4. Alsaidan SM, Alsughayer AA, Eshra AG. Improved dissolution rate of indomethacin by adsorbents. Drug Dev Ind Pharm 1998; 24 :389-94.
5. Wickstrom K. Acute bacterial conjunctivitis - benefits versus risks with antibiotic treatment. Acta Ophthalmol (Oxf) 2008; 86 :2-4.
6. Motwani SK, Chopra S, Talegaonkar S, Kohli K, Ahmad FJ, Khar RK. Chitosan - sodium alginate nanoparticles as submicroscopic reservoirs for ocular delivery: Formulation, optimisation and in vitro characterization. Eur J of Pharm Biopharm 2008; 68 :513–25.
7. Calvo P, Vila-Jato JL, Alonso MJ. Comparative *in vitro* evaluation of several colloidal systems, nanoparticles, nanocapsules and nanoemulsions as ocular drug carriers. J Pharm Sci 1996; 85 :530–6.
8. Vulovic N, Primorac M, Stupar M, Ford JL. Some studies into the properties of indomethacin suspensions intended for ophthalmic use. Int J Pharm 1989; 55 :123–8.
9. Muchtar S, Abdulrazik M, Frucht-Pery J, Benita S. Ex vivo permeation study of indomethacin from a submicron emulsion through albino rabbit cornea. J Control Release 1997; 44:55.
10. Nita LE, Chiriac AP, Nistor M. An in vitro release study of indomethacin from nanoparticles based on methyl methacrylate/glycidyl methacrylate copolymers. J Mater Sci: Mater Med 2010; 2 :3129-40.
11. Wongmekiat A, Yoshimatsu S, Tozuka Y, Moribe K, Yamamoto K. Investigation of drug Nanoparticulate Formation by Co-grinding with Ciclodextrins: Studies for Indometacin, Furosemide and Naproxen. J Incl Phenom Macro 2006; 56 :29-32.
12. Yamak HB. Emulsion Polymerization: Effects of Polymerization Variables on the Properties of Vinyl Acetate Based Emulsion Polymers. In: Dr. Faris Yılmaz, editor. Polymer sciences. InTech; 2013. p. 35-70.
13. Herk A. Chemistry and Technology of Emulsion Polymerization. Oxford: Blackwell Publishing; 2005.
14. Chern CS. Emulsion Polymerization Mechanisms and Kinetics. Prog Polym Sci 2006; 31 :443-86.
15. Andonova V, Georgiev G, Toncheva V, Kassarova M. Preparation and study of poly(vinyl acetate) and poly(styrene) nanosized latex with indometacin. Pharmazie 2012; 67(7) :601-4.
16. Andonova V, Georgiev G, Toncheva V, Petrova N, Kassarova M. Nanoparticles with indometacin – drug delivery systems for ocular administration. Folia Medica 2013; 55(1) :76-82.
17. Kostova B, Kamenska E, Momekov G, Rachev D, Georgiev G, Balashev K. Synthesis and characterization of novel drug delivery nanoparticles based on polyzwitterionic copolymers. Eur Polym J 2013; 49 :637-45.

18. Kostova B, Kamenska E, Rachev D, Simeonova S, Georgiev G, Balashev K. Polyzwitterionic copolymer nanoparticles loaded *in situ* with metoprolol tartrate: synthesis, morphology and drug release properties. J Polymer Res 2013; 20:60.
19. Ibrahim MM, Abd-Elgawad HAE, Soliman OAE, Jablonski M. Natural bioadhesive biodegradable nanoparticles-based topical ophthalmic formulations for sustained celecoxib release: In vitro Study. JPTDR 2013.
20. Budhian A, Siegel SJ, Winey KI. Controlling the in vitro release profiles foe a system of haloperidol-loaded PLGA nanoparticles. Int J Pharm 2008; 346 :151-9.
21. Tzankov B, Yoncheva K, Popova M, Szegedi A, Momekov G, Mihaly J et al. Indometacin loading and in vitro release properties from novel carbopol coated spherical mesoporous silica nanoparticles. Micropor Mesopor Mat 2013; 171 :131-8.
22. Martena V, Censi R, Hoti E, Malaj L, Di Martino P. Indomethacin nanocrystals prepared by different laboratory scale methods: effect on crystalline form and dissolution behavior. J Nanopart Res 2012; 14 :1275.
23. Mokarram RA, Kebriaee zadeh A, Keshavarz M, Ahmadi A, Mohtat B. Preparation and in-vitro evaluation of indomethacin nanoparticles. DARU 2010; 18(3).
24. Zlatkov A, Peikov P, Obreshkova D, Pencheva I. Spectral analyses methods for chemical compounds. Plovdiv: Macros; 2010.
25. Gebremichael E. Pharmaceutical Eutectics: Characterization and Evaluation of Tolbutamide and Haloperidol using Thermal Analytical and Complementary Techniques, [Thesis for PhD degree], University of Toledo, College of Pharmacy; 2010.
26. Kostova B. Development and characterization of matrix systems, based on new synthesized zwitterionic copolymers, [Thesis for PhD degree], Medical University–Sofia, Faculty of Pharmacy; 2008.
27. Nagarwal RC, Kant S, Singh PN, Maiti P, Pandit JK. Polymeric nanoparticle system: A potential approach for ocular drug delivery. J Control Release 2009; 136 :2-13.
28. Gonzales-Mira E, Egea MA, Garcia ML, Souto EB. Design and ocular tolerance of flurbiprofen loaded ultrasound-engineered NLC. Colloid and Surfaces B: Biointerfaces 2010; 81 :412-21.
29. Singhvi G, Mahaveer S. In-vitro drug release characterization models. IJPSR 2011; II(I) :77-84.
30. Collett J, Moreton R. Formulation of modified-release dosage forms. In: Aulton M, editor. Aulton's Pharmaceutics. 3rd ed. Churchill Livingstone Elsivier; 2007. p. 487-95.
31. Yang Z, Huck W, Clarke SM, Tajbakhsh A, Terentjev E. Shape-memory nanoparticles from inherently non-spherical polymer colloids. Nature Materials 2005; 4.
32. Ramaile H. Structure-property relationships in the Design, Assembly, Applications. ProQuest; 2004. p. 1-19.
33. Carraher C, Seymour R. Seymour/Carraher's polymer chemistry. Taylor & Francis, editors. CRC Press; 2003. p. 43–5.